https://doi.org/10.5194/egusphere-2026-1391
Preprint. Discussion started: 8 May 2026

Multi-dimensional, Multi-Constraint Seismic Inversion of Acoustic Impedance Using Fuzzy Clustering Concepts

Saber Jahanjooy[1,2], Hosein Hashemi[2], Majid Bagheri[2]
[1] Department op Petroleum Geosciences, Soran University, Soran, KRG, Iraq
[2] Institute of Geophysics, University of Tehran, Tehran, Iran

Correspondence to: Saber Jahanjooy (saber.jahanjooy@soran.edu.iq)

Abstract

Seismic inversion is a fundamental procedure that converts seismic data into useful information about underlying rock and fluid characteristics. However, because seismic data are band-limited, the inversion process is intrinsically difficult, resulting in non-unique solutions. To overcome these issues, several constraints are used to enforce properties such as smoothness and sparsity on the inversion results. We propose a technique that includes the clustering properties of previous information, such as well logs and geological data, into the inversion process. This grouping helps to preserve geological continuity and improves the resolution of the inversion data. By incorporating this strategy into our inversion framework, we can better describe the subsurface and deliver more consistent findings. Our technique was evaluated on both synthetic and actual seismic data, confirming its ability to generate accurate acoustic impedance models. Furthermore, the approach generated deconvolved and denoised versions of the seismic data, which are useful for future interpretation. The membership sections generated by the inversion method also demonstrated considerable promise for tracing geological horizons, discriminating between distinct sequences and layers, and even predicting likely layer contents. In conclusion, this work proposes an upgraded seismic inversion approach that utilizes the ability of clustering to incorporate earlier geological knowledge, resulting in more accurate and interpretable findings.

https://doi.org/10.5194/egusphere-2026-1391
Preprint. Discussion started: 8 May 2026

1 Introduction

Seismic sections are bandlimited data that manifest a general overview of the structural scheme of the subsurface layers. However, post-processing steps and analysis reveal more comprehensive information on the geophysical properties and contents of these layers. Seismic inversion creates models of subsurface properties such as acoustic impedance from seismic traces. These models are the source of our information on petrophysical properties and reservoir characterizations (Gogoi and Chatterjee, 2019, Jafri et al., 2017). The vital applications of these models from seismic inversion in seismic interpretation and hydrocarbon exploration attract the attention of scientists to develop effective and efficient seismic inversion methods.

Numerous seismic inversion methods have been introduced by researchers. These methods can be categorized based on the processing step of the input seismic data (pre-stack and post-stack), the supporting data (Blind and model-based), the mathematical calculations (deterministic and statistical, and the assumptions on the results. The pre-stack seismic inversions use angle-stacked or offset-stacked seismic data and well-logs to create models of P-impedance, S-Impedance, Vp/Vs, or variations of Lame's parameters (Mallick, 1995, Goodway et al., 1997). These models could be used to interpret reservoirs, fluid contents, and rock properties (Vernik, 2016). However, pre-stack inversion needs high-quality seismic data with a good signal-to-noise ratio and accurate AVO or AVA analysis. It is also computationally expensive and time-consuming. Post-stack seismic inversions utilize the final stacked seismic sections to create a high-resolution acoustic impedance (AI) model of the subsurface (Maurya et al., 2020), which is related to lithology and porosity, but not directly to fluid content. Post-stack inversion is simpler and faster than pre-stack inversion, and it can produce higher-resolution images of the subsurface structures (Maurya and Singh, 2018).

Deterministic seismic inversions minimize the difference between seismic traces and synthetic traces from the created model while satisfying predefined constraint(s) (Cooke and Cant, 2010, Rosa et al., 2020). However, interpreting the results of these methods could be difficult due to the different vertical scale than true geological models and well logs and the limited frequency band of the result models (Francis, 2010, Rosa et al., 2022). In contrast, statistical inversions (Haas and Dubrule, 1994, Yu et al., 2020) use statistical properties of well-logs data and amplitudes of seismic data to build a model on spatial grids. This procedure covers the limited frequency bandwidth of the seismic data by using prior information. Another way to create broadband models is to use deterministic and statistical seismic inversion simultaneously (Fu, 2004).

Single trace inversion creates simple interpretable results (Yilmaz, 2001). However, the non-realistic assumption on density, band-limited, and low-resolution results make this method less applicable. Since seismic inversion is an ill-posed problem (Tarantola, 2005) and has non-unique solutions, studies try to reduce the possible solutions by adding constraints in the temporal-spatial domain or a transformation domain. For geophysical data and seismic inversion, in which the interpreter expects some behaviors in the final model, different types of constraints are commonly used. Tikhonov regularizations (Tikhonov et al., 1977) smooth the model (Li and Oldenburg, 1999), while total variation (Rudin et al., 1992) decreases the effects of outliers and noises while detecting sharp boundary changes. Blind seismic inversions add constraints to the inversion process and create models from seismic traces (Jahanjooy et al., 2022). Model-based inversions start from a low-frequency model from well-logs and seismic interpretations and create final models around the initial model (Cooke and Schneider, 1983)(She et al., 2019). An inverse optimization problem by try and error of different objective functions is a straightforward method to select an optimum objective function (Terekhov et al., 2010). Each of these constraints highlights one aspect of

https://doi.org/10.5194/egusphere-2026-1391
Preprint. Discussion started: 8 May 2026

the inversion model such as smoothness and ignores other aspects of the model such as step-wise transition of the layers.

Jointly inversion or parallel computing of other types of geophysical data is also used in creating geophysical models (Gyulai et al., 2013, Wang et al., 2024). This technique simultaneously calculates the geophysical models and overcomes the limitations of individual inversions by combining different types of data that are sensitive to different physical properties. As a result, this enhances the resolution and uniqueness of the inverted models and provides a more comprehensive interpretation (Zhdanov et al., 2012). Researchers have inverted seismic data with gravity, magnetotelluric, and other types of geophysical data (Le et al., 2016, Bennington et al., 2015, Rapstine, 2015, Liao et al., 2022). However, joint inversion could be computationally expensive, and sensitive to noise and uncertainties in the prior information. Moreover, integrating and linking different geophysical data and models could be challenging.

Modern machine learning algorithms allow the incorporation of seismic data, well logs, and geological data to create geophysical models (Liu, 2019, Barman and Sen, 2022). Machine learning seismic inversion aims to create models with higher resolution, faster convergence, better robustness, and less manual input (Chen and Saygin, 2021). Machine learning (ML) in seismic inversion has various advantages, including increased accuracy and efficiency by utilizing algorithms that can automatically learn complicated patterns from vast datasets (Zhang et al., 2021, Chen and Schuster, 2020). When compared to standard inversion approaches, machine learning algorithms can enhance resolution while reducing computing overhead. However, they also bring obstacles, such as the requirement for large, high-quality datasets to properly train models, potential overfitting of training data, and difficulty in understanding the findings (Yu and Ma, 2021). Furthermore, ML techniques may necessitate substantial computing resources, hyperparameter selection (Meng et al., 2021) and expertise to execute and evaluate.

In data science, the dimensionality and complexity of the data can be reduced by clustering. Similarly, geophysical methods use clustering to treat the data (Hashemi et al., 2008) and extract useful features and patterns from the data (Moosavi et al., 2023). Furthermore, clustering can impose structural or statistical constraints on models, thereby enhancing the resolution and robustness of inversion results. In seismic inversion, one of the most advantageous aspects of fuzzy clustering is its ability to integrate prior non-seismic data into the inversion process (Sun and Li, 2016). As noted by Sun (2016), the nonlinearity, uncertainty, and heterogeneity of subsurface structures and properties are effectively managed by incorporating fuzzy clustering terms into the inversion. Building on this concept, Kieu and Kepic (2020) extended the model-based Occam's inversion (Cooke and Schneider, 1983) and add a fuzzy term to incorporate petrophysical information in the inversion (Kieu and Kepic, 2020). However, in complicated geological settings where seismic impedance may not correlate well with petrophysical parameters, this expanded method—which depends on trustworthy borehole data and previous petrophysical constraints—may be insufficient. Furthermore, the choice of fuzzy clustering parameters and bias from the original model may have an impact on the outcomes.

This research proposes a multi-term objective function for seismic inversion. The aim is to integrate the prior geophysical data from well logs or from other geological sources, and seismic traces in the inversion process and deal with various constraints on the resulting model. The constraints include data fidelity, model perturbation, smoothness, sparsity, and clustering. Despite the complexity of the proposed objective function, it can be solved using established methods such as least squares or matching pursuit. Although the method is model-based, it has

https://doi.org/10.5194/egusphere-2026-1391
Preprint. Discussion started: 8 May 2026

less dependence on the initial model and wavelet. The proposed fuzzy seismic inversion creates a deconvolved reflectivity section, a denoised version of the seismic data, and membership sections, as well as the acoustic impedance model. The result membership sections from the inversion process indicate the degree of belonging of each data point to different rock types or facies and represent a novel concept with potential applications in seismic interpretation.

https://doi.org/10.5194/egusphere-2026-1391
Preprint. Discussion started: 8 May 2026

2 Theory

2.1 Data misfit

The physical properties of the subsurface are unknown, and the goal is to estimate these properties, from limited geophysical data through ill-posed optimizations. For the reflection seismic traces, $\boldsymbol{d}$ is the convolution result of seismic wavelets, $\boldsymbol{w}$ and reflectivity series, $\boldsymbol{r}$ ($\boldsymbol{d} = \boldsymbol{w} * \boldsymbol{r}$). If $\mathbf{W}$ is the convolution matrix of the wavelet then the seismic trace(s) are a multiplication of $\mathbf{W}$ and $\boldsymbol{r}$ ($\boldsymbol{d} = \mathbf{W}\boldsymbol{r}$). In other words, the data misfit is a linear relation of the trace(s) and reflectivity:

$$\boldsymbol{\Phi}_d = \|\boldsymbol{d} - \mathbf{W}\boldsymbol{r}\|_2^2. \tag{1}$$

where $\|.\|_2^2$ is the Frobenius (Euclidean) norm. Berteussen and Ursin (1983) have formulated the reflectivity for a continuous acoustic impedance media ($\mathbf{z}$) (Berteussen and Ursin, 1983):

$$\boldsymbol{r}_j = \frac{1}{2}\ln\left(\frac{\boldsymbol{z}_{j+1}}{\boldsymbol{z}_j}\right) = \frac{1}{2}\log(\boldsymbol{z}_{j+1}) - \frac{1}{2}\log(\boldsymbol{z}_j) = \boldsymbol{x}_{j+1} - \boldsymbol{x}_j. \quad (a)$$

$$\boldsymbol{r} = \boldsymbol{D}_v\boldsymbol{x}. \quad (b)$$

(2)

where $\boldsymbol{Z}_j$ is the acoustic impedance of the j[th] sample point, and $\boldsymbol{D}_v$ is the first-order differential matrix along the time dimension. Conversely, having $\boldsymbol{r}$, the value of x can be obtained in a recursive calculation using Eq. (3):

$$\boldsymbol{x}_{j+1} - \boldsymbol{x}_j = 2\sum_{i=1}^{j}\boldsymbol{r}_i. \quad (a)$$

$$\boldsymbol{x} = \boldsymbol{H}\boldsymbol{r}. \quad (b)$$

$$\boldsymbol{z}_j = \boldsymbol{z}_1 e^{2\sum_{i=1}^{J} r_j} = \boldsymbol{z}_1 e^{\boldsymbol{H}\boldsymbol{r}}. \quad (c)$$

$$\boldsymbol{r} = [r_1.r_2.\ldots.r_N]^T. \quad \boldsymbol{H} = \begin{bmatrix} 0 & 0 & \cdots & 0 \\ 2 & 0 & \cdots & 0 \\ 2 & 2 & \cdots & 0 \\ \vdots & \vdots & \ddots & \vdots \\ 2 & 2 & \cdots & 2 \end{bmatrix}.$$

(3)

2.2 Model perturbation

An initial guess could improve the uniqueness of the inversion model (Mallick, 1995). This guess usually is based on the well-logs and contains the general low-frequency trend of the subsurface model ($\boldsymbol{x}^{(0)}$). In model-based inversion methods, the final model is often a refinement or small perturbation around this initial guess. The relationship can be expressed as:

$$\boldsymbol{\Phi}_x = \left\|\boldsymbol{x}^{(0)} - \mathbf{H}\mathbf{r}\right\|_2^2. \tag{4}$$

The model-based inversion relies on the assumption that the initial model is reasonably close to the true subsurface structure. However, the effectiveness of this method heavily depends on the accuracy of the initial guess.

https://doi.org/10.5194/egusphere-2026-1391
Preprint. Discussion started: 8 May 2026

2.3 Sparsity

Another constraint to reduce the ill-posedness of the seismic inversion problem is the sparsity of the reflectivity. Sparsity encourages solutions in which the reflectivity series has few important non-zero coefficients, hence highlighting the most important elements in the seismic data. Because seismic data is band-limited, it can be challenging to identify high-frequency changes and thin-bed layers. However, by imposing sparsity, $\boldsymbol{\Phi}_r$, the inversion process becomes more competent at detecting these features. Because it prevents overfitting to noise, this constraint not only aids in the recovery of finer-scale geological features and sharper interfaces, but it also improves the stability and resilience of the inversion. Usually, the sparsity restriction is represented mathematically as follows:

$$\boldsymbol{\Phi}_r = |\boldsymbol{r}| \tag{5}$$

where $|\boldsymbol{r}|$ denotes the L1 norm of the reflectivity series.

2.4 Smoothness

A smoothness term, $\boldsymbol{\Phi}_s$, could enhance the consistency of optimizations like seismic inversion, especially in cases when gradual variations in the underlying structure are anticipated. Smoothness requirements are often employed, independent of noise level, to promote geologically plausible models and avoid artificial oscillations, however they are useful in noisy data situations as well. Considering the dimensions of the data and the model properties, the penalty term is defined as either the first or second derivative of the model along each dimension or a combination of these derivatives (Constable et al., 1987). Equation (6) lists a collection of smoothness objective functions that do not conflict with the sparsity of the reflectivity. $\boldsymbol{D_v}$ and $\boldsymbol{D}_h$ are the first-order differential matrix along the temporal and spatial dimension, respectively. The $\boldsymbol{\alpha}$ is a small factor that controls the smoothness variation along these directions.

$$\begin{aligned}
&\boldsymbol{\Phi}_s = \|\boldsymbol{D}_h\boldsymbol{x}\|_2^2 = \|\boldsymbol{D}_h\boldsymbol{Hr}\|_2^2. \quad (a)\\
&\boldsymbol{\Phi}_s = \|\boldsymbol{D}_h^2\boldsymbol{x}\|_2^2 = \|\boldsymbol{D}_h^2\boldsymbol{Hr}\|_2^2. \quad (b)\\
&\boldsymbol{\Phi}_s = \|\boldsymbol{D}_v\boldsymbol{D}_h\boldsymbol{x}\|_2^2 = \|\boldsymbol{D}_v\boldsymbol{D}_h\boldsymbol{Hr}\|_2^2 = \|D_h\boldsymbol{r}\|_2^2. \quad (c)\\
&\boldsymbol{\Phi}_s = \|\alpha\boldsymbol{D}_v\boldsymbol{x}\|_2^2 + \|\boldsymbol{D}_h\boldsymbol{x}\|_2^2 = \|\alpha\boldsymbol{D}_v\boldsymbol{Hr}\|_2^2 + \|\boldsymbol{D}_h\boldsymbol{Hr}\|_2^2 = \left\|\begin{pmatrix}\alpha\boldsymbol{D}_v\\ \boldsymbol{D}_h\end{pmatrix}\boldsymbol{Hr}\right\|_2^2. \quad (d)\\
&\boldsymbol{\Phi}_s = \|\alpha\boldsymbol{D}_v^2\boldsymbol{x}\|_2^2 + \|\boldsymbol{D}_h^2\boldsymbol{x}\|_2^2 = \|\alpha\boldsymbol{D}_v^2\boldsymbol{Hr}\|_2^2 + \|\boldsymbol{D}_h^2\boldsymbol{Hr}\|_2^2 = \left\|\begin{pmatrix}\alpha\boldsymbol{D}_v^2\\ \boldsymbol{D}_h^2\end{pmatrix}\boldsymbol{Hr}\right\|_2^2. \quad (e)\\
&\boldsymbol{\Phi}_s = \|\alpha\boldsymbol{D}_v\boldsymbol{x} + \boldsymbol{D}_h\boldsymbol{x}\|_2^2 = \|(\alpha\boldsymbol{D}_v + \boldsymbol{D}_h)\boldsymbol{Hr}\|_2^2. \quad (f)\\
&\boldsymbol{\Phi}_s = \|\alpha\boldsymbol{D}_v^2\boldsymbol{x} + \boldsymbol{D}_h^2\boldsymbol{x}\|_2^2 = \|(\alpha\boldsymbol{D}_v^2 + \boldsymbol{D}_h^2)\boldsymbol{Hr}\|_2^2. \quad (g)
\end{aligned} \tag{6}$$

To extend the algorithm to three dimensions, instead of $\boldsymbol{D}_h$ in the smoothness term, one can simply use $\boldsymbol{D}_x$ and $\boldsymbol{D}_y$, which are the first difference matrices along the inline and crossline directions.

2.5 Clustering

Generally, a subsurface geological medium consists of different segments, sequences, or layers. Clustering assigns similar points of the subsurface model to distinct groups. Hard clustering methods such as K-means assume that

https://doi.org/10.5194/egusphere-2026-1391
Preprint. Discussion started: 8 May 2026

each data point belongs to an exclusive group that has a calculated cluster center or centroid (Han and Kamber, 2006). For a set of data points, x_j and centroids, o_k, K-means minimizes the objective function in Eq. (7):

$$\Phi_{c\,(KM)} = \sum_{j=1}^{M}\sum_{k=1}^{C} v_{jk} d_{jk}^2 \qquad (7)$$

where $\boldsymbol{d}_{jk}$ is the distance between a data point and its respective centroid. $\boldsymbol{v}_{jk}$ is 1 if $\boldsymbol{x}_j$ belongs to cluster k, and 0 otherwise.

Unlike hard clustering, which allows data points to belong to only one group, soft or fuzzy clustering allows data points to belong to multiple groups with relative memberships. A fuzzy clustering method such as Fuzzy C-Means, calculates the centroids $\boldsymbol{o}_k$ of the clusters and the normalized memberships $\boldsymbol{u}_{jk}$ of each data point to these centroids in an iterative process. As in the K-means, FCM aims to minimize the objective function in Eq. (8) (Bezdek, 2013):

$$\boldsymbol{\Phi}_{c\,(FCM)} = \sum_{j=1}^{M}\sum_{k=1}^{C} \boldsymbol{u}_{jk}^{q} \boldsymbol{d}_{jk}^2. \qquad (8)$$

where q is a parameter that indicates the fuzziness of the data, which controls the degree of cluster overlap, with higher values of q leading to more overlap and softer clustering boundaries. C represents the number of clusters within the data. Depending on the primary assumptions about the shapes of the clusters, distances can be in various forms such as Euclidian (Eq. (9)) as in FCM or Mahalanobis (Mahalanobis, 2018) as in Gustafson Kessel (GK) fuzzy clustering (Krishnapuram and Kim, 1999).

$$\boldsymbol{d}_{jk}^2 = \left\|\boldsymbol{x}_j - \boldsymbol{o}_k\right\|_2^2. \qquad (9)$$

The clustering objective function in the Eq. (8) has two variables, $\boldsymbol{u}$, and $\boldsymbol{O}$. To solve for each variable, one needs to differentiate the objective function for one of these variables while the other variable is treated as known and set the resulting expressions to zero (Zadeh, 1965). Starting with an initial guess for centroids, the centroids and memberships are updated in an iterative process:

$$\boldsymbol{u}_{jk} = \frac{1}{\sum_{i=1}^{C}\left(\frac{\boldsymbol{d}_{jk}}{\boldsymbol{d}_{ji}}\right)^{\frac{2}{q-1}}}. \quad (a)$$

$$\boldsymbol{O}_k = \frac{\sum_{j=1}^{M} \boldsymbol{u}_{jk}^{q}\, \boldsymbol{x}j}{\sum_{j=1}^{M} \boldsymbol{u}_{jk}^{q}}. \quad (b)$$

(10)

Using proper distance calculation modifies the clustering results to the behaviour of the input data (Krishnapuram and Kim, 1999). On the other hand, spatial properties such as stepwise or smooth transition within each cluster are addressed in several fuzzy clustering research. In the revised fuzzy clustering methods, spatial information is

https://doi.org/10.5194/egusphere-2026-1391
Preprint. Discussion started: 8 May 2026

incorporated into the clustering process (Pham, 2001, Li et al., 2011, Chuang et al., 2006). To account for the probable correlation of the data points to their neighbouring, Chuang et al (2006) add the local behaviour of the clusters (h) in windowed areas around the calculated data point (Chuang et al., 2006):

$$\boldsymbol{h}_{jk} = \sum_{l \in L} \boldsymbol{u}_{lk} \quad (11)$$

Where L is the indices collection for the neighbouring window $\boldsymbol{x}_j$. In this case, the membership will be updated by using Eq. (12) where the β and γ parameters control the contribution of $\boldsymbol{u}$ and $\boldsymbol{h}$. Knowing that the u_j is normalized, when $\beta = 1$ and $\gamma = 0$, $u'_{jk}$is equal to $\boldsymbol{u}_{jk}$.

$$u'_{jk} = \frac{\boldsymbol{u}_{jk}^{\beta} \boldsymbol{h}_{jk}^{\gamma}}{\sum_{i=1}^{C} \boldsymbol{u}_{ji}^{\beta} \boldsymbol{h}_{ji}^{\gamma}} \quad (12)$$

A main concern in the clustering process is the optimum number of clusters. Elbow methods are widely used for determining the optimum number of clusters (Bezdek and Pal, 1998). Here, well-data are used to estimate the cluster number. Although this information gives valuable insight into the overall model, the problem arises when the clusters of the well-site do not exist in the other location or conversely, there are additional clusters in the subsurface. The later problem could also arise when windowing the seismic data to smaller sub-sections. In this particular scenario, there may be a smaller number of clusters in each window. The large numbers of pre-defined clusters overlap, and/or there are clusters in which all of their memberships are relatively small. To address this challenge and avoid the use of the elbow method for each windowed data, a Gram matrix is created (Horn and Johnson, 2012):

$$\mathrm{G} = \boldsymbol{u}^T \boldsymbol{u} \quad (13)$$

Data points have small memberships to the centroids which are far from the window data. Therefore, the diagonal elements related to these clusters in the Gram matrix are small. On the other hand, the centroids which have high overlap, create large non-diagonal elements. Omitting the highly overlapped clusters and the clusters which have negligible memberships, optimizes the number of clusters in the windowed data.

2.6 Seismic inversion

Equation (1) has non-unique answers. Adding a model perturbation term ($\boldsymbol{\Phi}_x$) keeps the resulting model close to the initial low-frequency guess, while the sparsity term ($\boldsymbol{\Phi}_r$) tries to enhance the resolution of the data. The smoothness term $\boldsymbol{\Phi}_s$ considers the spatial-temporal properties of the resulting model. A clustering term $\boldsymbol{\Phi}_c$ forces the model to satisfy initial information, as cluster centroids and extend of the clusters, on the model. This information could come from well-logs, seismic interpretation, and/or geological settings. To decrease ambiguities of the result, all of the mentioned terms are considered and a multi-term objective function is created:

$$r = argmin_r\{\boldsymbol{\Phi}\} = argmin_r \left\{ \frac{w_d \boldsymbol{\Phi}_d}{\theta(d)} + \frac{w_x \boldsymbol{\Phi}_x}{\theta(x)} + \frac{w_s \boldsymbol{\Phi}_s}{\theta(c)} + \frac{w_c \boldsymbol{\Phi}_c}{\theta(c)} + \boldsymbol{\Phi}_r \right\}.$$

https://doi.org/10.5194/egusphere-2026-1391
Preprint. Discussion started: 8 May 2026

$$\theta(d) = \frac{norm(\boldsymbol{d}.2)}{length(\boldsymbol{d})}. \quad \theta(\boldsymbol{x}) = \frac{norm(\boldsymbol{x}.2)}{length(\boldsymbol{x})}. \quad \theta(c) = \frac{norm(\boldsymbol{u}^q\,\hat{O}.2)}{length(\boldsymbol{x}) \times C} \tag{14}$$

To normalize contribution of the terms, each objective term is weighted using a denominator, $\theta(\cdot)$. The $norm(\boldsymbol{d}.2)$ is the Euclidian norm. $\hat{O}$ is a stack of identical copies of O with its size equal to the memberships, $\boldsymbol{u}$. To simplify the objective function, and account for the range of values in the model and its clusters, and after examining practical examples, the same θ is used for both the smoothing and clustering terms. Weighting factors balance the misfit or data fidelity term and the other terms (such that $w_d + w_x + w_s + w_C = 1$). This eliminates the need for high dimensional L-curve (Brooks et al., 1999), L-surface (Brooks et al., 1999), or Generalized cross-validation (Golub et al., 1979) methods to find optimum regularization parameters.

Various forms of hard or soft clustering may be employed as the clustering term. To solve Eq. (14), $\boldsymbol{\Phi}$ is rearranged as a conventional L2-L1 problem in the Eq. (15). Common methods such as the iterative reweighted least square (IRLS) or the orthogonal matching pursuit (OMP) may be employed to solve this new objective function.

$$\boldsymbol{\Phi} = \|\mathbf{A}\mathbf{r} - \boldsymbol{b}\|_2^2 + |\boldsymbol{r}|.$$

$$\hat{\boldsymbol{d}} = \begin{bmatrix} d_1 \\ d_2 \\ \vdots \\ d_N \end{bmatrix}. \quad \hat{\boldsymbol{x}}_0 = \begin{bmatrix} x_1 \\ x_2 \\ \vdots \\ x_M \end{bmatrix}. \quad \hat{I} = \begin{bmatrix} 0 \\ 0 \\ \vdots \\ 0 \end{bmatrix}. \quad \hat{U} = \begin{bmatrix} diag\left\{\sqrt{\boldsymbol{u}_1^q}\right\} \\ diag\left\{\sqrt{\boldsymbol{u}_2^q}\right\} \\ \vdots \\ diag\left\{\sqrt{\boldsymbol{u}_C^q}\right\} \end{bmatrix}. \quad \hat{UO} = \begin{bmatrix} \left\{\sqrt{\boldsymbol{u}_1^q}\right\} o_1 \\ \left\{\sqrt{\boldsymbol{u}_2^q}\right\} o_2 \\ \vdots \\ \left\{\sqrt{\boldsymbol{u}_C^q}\right\} o_C \end{bmatrix}.$$

$$\hat{\boldsymbol{W}} = \begin{bmatrix} W & & \\ & \ddots & \\ & & W \end{bmatrix}. \quad \hat{\boldsymbol{H}} = \begin{bmatrix} H & & \\ & \ddots & \\ & & H \end{bmatrix}, \boldsymbol{A} = \begin{bmatrix} w_1\hat{\boldsymbol{W}} \\ w_2\hat{\boldsymbol{H}} \\ w_4\hat{\boldsymbol{D}} \\ \sqrt{w_5}\hat{\boldsymbol{U}} \end{bmatrix}. \quad \boldsymbol{b} = \begin{bmatrix} w_1\hat{\boldsymbol{d}} \\ w_2\hat{\boldsymbol{x}}_0 \\ \hat{I} \\ \sqrt{w_5}\hat{UO} \end{bmatrix}$$

(15)

which u_i represents the memberships to the i[th] centroid. Having seismic data, wavelet, initial model, and prior clustering information, Eq. (15) solves for reflectivity. Equation (3) uses this reflectivity and creates an impedance model.

Solving Eq. (10) for memberships and centroids and repeating the inversion converges the model, the centroids, and the memberships. In clustering methods, the centroids and memberships are updated repeatedly until they converge. However, here these updates happen just once per each iteration of the inversion using Eq. (10) and Eq. (14). You can opt to update the centroids and memberships based solely on the model, ($[\boldsymbol{x}]$) or include both the time (depth) of data points and the model, ($[\boldsymbol{t}.\boldsymbol{x}]$).

Algorithm 1 summarizes the procedure of the above Multi-Objective Fuzzy Seismic Inversion (MFSI). The workflow begins with the input of post-stack seismic data, well data (density, sonic, check-shot, and well-tops), and other petrophysical data. Data preparation involves horizon interpretation and seismic well-tie. An initial model is constructed using the interpreted horizons and well-tie results, with optional geological boundary definition. Fuzzy clustering is applied to well and petrophysical data to compute prior cluster centers when necessary. The MFSI algorithm integrates these inputs to produce outputs, including an acoustic impedance model, updated cluster centers, membership sections, and a reflectivity or deconvolved section.

https://doi.org/10.5194/egusphere-2026-1391
Preprint. Discussion started: 8 May 2026

Algorithm 1: Multi-Objective Fuzzy Seismic Inversion, MFSI workflow

1 **Input Data**:
- Processed post-stack seismic data.
- Well-data (density, sonic, check-shot, well-top).
- Other petrophysical data.

2 **Data Preparation:**
- Perform horizon interpretation.
- Conduct seismic-well tie.

3 **Initial Model Construction**:
- Generate an initial model using horizon interpretation and seismic-well tie results.
- Define geological boundaries using the initial model and well data (optional).

4 **Fuzzy Clustering Analysis:**
- Apply fuzzy clustering to well-data and petrophysical data to compute prior cluster centers (optional).

5 **Fuzzy Seismic Inversion**:
- Apply the MFSI on the seismic data and other available data.

6 **Output Results:**
- Acoustic impedance model,
- Updated cluster centers,
- Membership sections,
- Reflectivity or de-convolved section,

https://doi.org/10.5194/egusphere-2026-1391
Preprint. Discussion started: 8 May 2026

3 Application Examples

The proposed method is applied to a synthetic seismic section and an inline section of the F3 block data set. The basic structure of the synthetic model allows us to observe the results in common 1D and 2D cases. The complex structures in the F3 data and the presence of hydrocarbons in the North Sea make the inversion process more challenging.

3.1 Synthetic example

Figure 1a shows a synthetic geological model that consists of six major geological segments. A seismic section is created by convolving a Ricker wavelet and the reflectivity of the synthetic model. The signal-to-noise ratio of the created data with a 30 Hz dominant frequency is 1dB (Figure 1b). The true model is smoothed along vertical and lateral directions (Figure 1c) and the result is used as an initial model.

Prior information such as the number and quantities of the main model clusters are usually attainable using clustering of the well-data and well-logs. However, for the synthetic model, the segment's AI is available and the cluster number, C is equal to 4. The proposed objective function could employ different clustering approaches (Φ_c) as well as various smoothness terms (Φ_s). **Figure 2** shows normalized mean square errors (NMSE) for the results of the inversion, while K-means and FCM are used as the clustering term. 1D stands for when each trace is inverted separately. The second case is when the smoothness term in two-dimensional data is not used. For the 2D cases, in which neighbouring traces are considered, the calculation bins are windows of three traces. Although the input seismic data has high noise level, both clustering approaches have relatively small errors. However, the NMSE of fuzzy-based inversions are smaller. As an example, Figure 3 shows the resulting model when the clustering term is fuzzy and the smoothness is as Eq. (7b). Despite the high noise level, the main cluster regions are separated.

Model-based inversions converge around the low-frequency initial models. Errors in the initial model remain in the final result. However, forcing the result to obey the clustering term moves the model toward its true value. Figure 3c displays an inversion result which, compared to Figure 3b, is started from a smoother and smaller initial model. However, the inversion result converged toward the true model.

Data fidelity term ($\boldsymbol{\Phi}_d$) uses a known wavelet to estimate the seismic response of the reflectivity series. Incorrect wavelets lead to miscalculations and incorrect models. To check the dependence of the inversion results on the wavelet, the used Ricker zero phase wavelet is rotated. One trace of the synthetic section is inverted using different rotated Ricker wavelets. NMSE of the results are presented in Figure 4. Compared to the true zero-phase wavelet, a wide range of incorrect rotated wavelets create models which have NMSE comparable to the true wavelet.

Due to the low sensitivity of the proposed method to the noise level and the wavelet, the deconvolved traces are reliable. This could be seen in Figure 5 where the resulting reflectivity of trace 100 is compared to the true reflectivity. The reflectivity of the main boundaries is recovered. Although some small random artificial spikes are created, this does not affect the lateral continuity of the layers (Figure 3a). Consequently, the synthetic trace created by using the resulting reflectivity is significantly de-noised (Figure 5).

3.2 Real case example

A Seismic inline section of the Netherlands OpendTect F3 dataset which intersects F034 well is presented in Figure 6a. Five of the main seismic horizons are interpreted. The elbow method for Gustafson-Kessel clustering

https://doi.org/10.5194/egusphere-2026-1391
Preprint. Discussion started: 8 May 2026

of impedance well log suggests 11 clusters in the sampled depth. However, the seismic horizons show six general facies segments (Chevitarese et al., 2018) and some sublayers. Although, it is not necessarily required, we preferred to use Gustafson-Kessel in the clustering of the well-logs. Gustafson-Kessel is adaptable to clusters of various forms and sizes. This versatility is critical in geophysical applications, since subsurface features are frequently complicated and irregular. A seismic wavelet is created by statistical wavelet estimation. The initial low-frequency model is created using Hampson-Russel software and the inversion bins are windows of three traces.

Four different scenarios are tested. In the first scenario, the initial model and centroids are available. Usually, well-logs provide some general properties of the model. Otherwise, the initial model can be created by using interpreted horizons, migration velocity, or other geophysical data. In the second scenario, assuming no clustering information, the initial model is clustered to create initial centroids for the inversion process. In a less probable case, for the third scenario, the initial model is not available or it is not created accurately but there is trusted initial clustering information. In this case, the inversion starts without the model perturbation term. The resulting model is used as the initial model for the next iterations and it updates at each iteration. The fourth scenario assumes no initial model and clustering information. In this case, the inversion starts without the model perturbation and clustering terms. The resulting model is the starting initial model and clustering source for the next iteration, which uses all of the objective terms. In reality, the initial model and clustering of an inversion bin can be used as initial information for the neighbouring bins.

On the other hand, in the inversion iterations, four different approaches can be used to update the centroids. In the first approach, the centroids only have one dimension, AI. While the magnitudes of the centroids are fixed, the memberships update at each iteration. The second approach also considers the time of the fixed centroids. In the third approach, the one-dimensional AI of the centroids and their memberships update at each iteration. The fourth approach updates both the magnitude and time of the centroids.

The proposed method, when it uses Eq. (7d) as smoothness, and C is equal to 6, is applied to the seismic section. The centroids are calculated using sonic and density logs at the location of the crossline 1008. As in approach two, only the memberships are updated. Although it is not a vital requirement, to reduce the number of iterations, it is recommended to start the inversion from the well-site location and use the memberships of the previous bin as a trusted initial membership for the neighbouring bins. While the fuzziness, q is equal to 2, the objective function converges after three iterations, ,Figure 6b and Figure 6c display the inversion results of the proposed method and model-based inversion of Hampson-Russel (HR) software, respectively. Although the models are analogous, the MFSI model has higher vertical and horizontal resolution and creates higher lateral continuity of the events.

The AI log derived from the density and sonic logs of the F034 well in the F3 Block is displayed in Figure 7a. In the left plot, the result of the model-based inversion closely follows the initial model, whereas the FSI result in the right plot deviates more. The AI created by the FSI aligns more with the AI log at the well location (Table 1), with an NMSE of 0.041 compared to 0.050 for the model-based method. Due to an error in the time-depth correction of the well-logs, there is an inconsistency from 1.5s to the end. A neighbouring trace to this well, located at the intersection of inline 441 and crossline 1008, is compared to the synthetic seismogram obtained by convolving the wavelet and reflectivity of the resulting inversion models (in Figure 7b). Compared to the model-based result, the synthetic seismogram of the FSI matches well with the original seismic trace, and the NMSE is

https://doi.org/10.5194/egusphere-2026-1391
Preprint. Discussion started: 8 May 2026

relatively small (Table 1). Typically, in the model-based inversion method, reducing data misfit comes at the cost of increasing errors in model estimation. However, as shown in Table 1, this is not the case for the FSI.

Table 1: NMSE of the AI and the synthetic traces from Model-based Inversion and FSI at the location of well log F034.

	AI Model	Synthetic Trace
Model-Based	0.050	0.876
FSI	0.041	0.282

In addition to the AI model, the inversion creates membership of each model point to each cluster center. Membership sections are sections with the dimensionality of the model in which each data point is the membership to one of the centroids. If there are C clusters, C separate membership sections will be created in which each section is a display of belonging of the model points to one of the cluster centers. These membership sections help to track and interpret the data. The membership sections created in the inversion process of Figure 6a, are displayed in the top row of Figure 8. Note that for all the images the colour range is 0 to 1. For simplicity of the figure plots, the axis of these sections is not shown here. As they match the interpreted horizons in Figure 6a, these membership sections can be used to interpret and track horizons. The main sequences are distinguished. Furthermore, the within-boundary variations of the model can be perceived and comprehended.

In another attempt, the fuzziness, q in the clustering term is set to 1.1 and the inversion is repeated. The result membership sections are displayed in the lower row of Figure 8. As is expected from the fuzzy clustering concept, the lower fuzziness tends the fuzzy clustering toward hard clustering and decreases the resolution of the membership sections.

To illustrate the range of possibilities, we applied all approaches from the first scenario and the fourth approach from each of the other scenarios across different inversion processes. The result membership sections comparable to the third membership in Figure 8 are displayed in Figure 9. The first approach (Figure 9a) unveils a detailed insight into the distribution of model magnitude in the subsurface. The second approach (Figure 9b) creates smoother cluster centers that track the fine impedance zones. However, the third approach creates more continuous and sharp results (Figure 9c). As in approach two, the fourth approach (Figure 9d) distinguishes sequences or layers of the subsurface. Nevertheless, it enhances the imprecise initial cluster data and has more lateral continuity. Figure 9e, f, and g display the membership section resulting from approaches two to four respectively while updating AI and times of the centroids. Although these approaches do not have all or part of the initial information, they create results comparable to the first approaches with less resolution.

In a different calculation, the elbow method on the well-log estimates 11 clusters as the optimum cluster number and creates centroids. The result membership sections of the inversion process are displayed in Figure 10. Although finer variations of the memberships are created, in some regions the membership sections have a high correlation with other membership sections.

https://doi.org/10.5194/egusphere-2026-1391
Preprint. Discussion started: 8 May 2026

4 Discussion

The results of ill-posed problems such as seismic inversion greatly benefit from initial knowledge of the result. Adding additional constraints on the result decreases the ambiguity of the results and increases their uniqueness. The proposed MFSI algorithm aims to add multiple constraints to the inversion process. As a vital term of the MFSI, fuzzy clustering of known data influences the inversion result. The objective function of the MFSI has five terms and solving it using traditional ways can be challenging. The proposed weighting parameters have eased the process of determining optimal regularization parameters (Eq. (14)). By default, all weights are set equally, but the operator can adjust them according to the reliability of each respective term. For instance, when seismic data has a higher SNR, the weight assigned to the data fidelity term can be increased. This adjustment also applies to the initial model and prior clustering data. Equation (15) simplifies the multi-term objective function to a common norm one problem.

The examples (Figure 3) show that the data fidelity term of the proposed fuzzy seismic inversion ensures that the synthetic seismic data from the resulting model is close to the input seismic data. The model perturbation term is a guarantee that the resulting model obeys a provided low-frequency model of the subsurface. This could convey the possible errors in the initial model to the resulting model. Depending on the expected behaviour of the subsurface and to account for lateral or vertical variations in the subsurface, the different provided smoothness terms could be examined. The sparsity constraint on the seismic reflectivity is an effort to achieve high vertical resolution. Usually, well-log data, geological sections of the subsurface, other geophysical methods, or seismic interpretation create a general view of the subsurface sequences or layers which could be used as prior information through the use of the clustering term.

The multi-objectiveness of the MFSI reduces the dependency of the results on the errors in the initial data (Figure 3 and Figure 4). MFSI uses a fixed wavelet in all of its iterations. Although the algorithm allows small errors in the wavelet, further research to update the wavelet at each iteration can improve the result. For situations such as non-stationary wavelets along time direction, and variation of the wavelet along spatial direction, the mentioned low-affection of the result by the wavelet is important. Some researchers propose to use the time-varying wavelet in the seismic inversion and improve the result (van der Baan, 2008, Zhang and Fomel, 2017).

The MFSI creates membership sections, as well as acoustic impedance sections (Figure 8). Based on the available data and assumptions on the cluster centers, one can compute the centroids and membership sections in four different scenarios, each using one of four possible approaches. The flexibility of the memberships sections (Figure 9 and Figure 10) makes them a valuable source for the interpreters and researchers to track horizons, distinguish sequences and layers, and identify possible contents of the layers. Here, the fuzziness is selected as 2. Decreasing the fuzziness shifts the fuzzy clustering toward hard clustering (Figure 8). However, the MFSI would benefit from further research on selecting the optimal fuzziness in its clustering term.

https://doi.org/10.5194/egusphere-2026-1391
Preprint. Discussion started: 8 May 2026

5 Conclusion

This research introduces a multi-objective fuzzy seismic inversion method based on different constraints to create an impedance model from post-stack seismic data. The proposed objective function is a combination of five well-known objective functions, each of which ensures a desired property in the resulting model. A simple solution to the new objective function is presented. Numerical synthetic and real data examples demonstrate the effectiveness of the proposed method in inverting seismic data. Although the method is model-based, the numerous constraints on the result make the proposed method less dependent on the initial data. Therefore, the reflectivity section generated by the algorithm is a reliable deconvolved result and it can create a denoised version of the input seismic data. The clustering term is a vital part of the inversion process. Examples showed that in this form of the proposed method, fuzzy clustering creates more reliable results than hard clustering. The resulting membership sections of the inversion help the interpreters track horizons, distinguish sequences and layers, and identify possible contents of the layers. However, the examples demonstrate that the initial clustering parameters, such as the number of clusters, significantly influence the final model and its interpretation. Moreover, the iterative nature of the inversion and clustering process introduces additional computational costs to the method. Further research on the initial wavelet, the optimal fuzziness, and the applications of membership sections is recommended. In summary, this research proposes a novel and robust seismic inversion method that can produce high-quality impedance models with various desirable features and facilitate the interpretation of seismic data.

https://doi.org/10.5194/egusphere-2026-1391
Preprint. Discussion started: 8 May 2026

Author contributions

Saber Jahanjooy developed the methodology, conducted the practical work, and wrote the initial manuscript. Hosein Hashemi and Majid Bagheri supervised the overall project and reviewed the manuscript.

Funding

The authors declare that no funds, grants, or other financial support were received during the preparation of this manuscript.

Data Availability

The real seismic data used in this study is from the F3-Demo-2020 dataset, which is publicly available at TerraNubis (https://terranubis.com/datainfo/F3-Demo-2020).

Competing Interests

The contact author has declared that none of the authors has any competing interests.

https://doi.org/10.5194/egusphere-2026-1391
Preprint. Discussion started: 8 May 2026

References

BARMAN, D. & SEN, M. Seismic inversion with dictionary learning using unsupervised machine learning. SEG International Exposition and Annual Meeting, 2022. SEG, D011S009R004.

BENNINGTON, N. L., ZHANG, H., THURBER, C. H. & BEDROSIAN, P. A. 2015. Joint inversion of seismic and magnetotelluric data in the Parkfield Region of California using the normalized cross-gradient constraint. *Pure and Applied Geophysics,* 172**,** 1033–1052.

BERTEUSSEN, K. & URSIN, B. 1983. Approximate computation of the acoustic impedance from seismic data. *Geophysics,* 48**,** 1351–1358.

BEZDEK, J. C. 2013. *Pattern recognition with fuzzy objective function algorithms*, Springer Science & Business Media.

BEZDEK, J. C. & PAL, N. R. 1998. Some new indexes of cluster validity. *IEEE Transactions on Systems, Man, and Cybernetics, Part B (Cybernetics),* 28**,** 301–315.

BROOKS, D. H., AHMAD, G. F., MACLEOD, R. S. & MARATOS, G. M. 1999. Inverse electrocardiography by simultaneous imposition of multiple constraints. *IEEE Transactions on Biomedical Engineering,* 46**,** 3–18.

CHEN, Y. & SAYGIN, E. 2021. Seismic inversion by hybrid machine learning. *Journal of Geophysical Research: Solid Earth,* 126**,** e2020JB021589.

https://doi.org/10.5194/egusphere-2026-1391
Preprint. Discussion started: 8 May 2026

CHEN, Y. & SCHUSTER, G. T. 2020. Seismic inversion by Newtonian machine learning. *Geophysics,* 85**,** WA185–WA200.

CHEVITARESE, D., SZWARCMAN, D., SILVA, R. M. D. & BRAZIL, E. V. 2018. Seismic facies segmentation using deep learning. *AAPG Annual and Exhibition,* 405.

CHUANG, K.-S., TZENG, H.-L., CHEN, S., WU, J. & CHEN, T.-J. 2006. Fuzzy c-means clustering with spatial information for image segmentation. *computerized medical imaging and graphics,* 30**,** 9–15.

CONSTABLE, S. C., PARKER, R. L. & CONSTABLE, C. G. 1987. Occam's inversion: A practical algorithm for generating smooth models from electromagnetic sounding data. *Geophysics,* 52**,** 289–300.

COOKE, D. & CANT, J. 2010. Model-based seismic inversion: Comparing deterministic and probabilistic approaches. *CSEG Recorder,* 35**,** 29–39.

COOKE, D. A. & SCHNEIDER, W. A. 1983. Generalized linear inversion of reflection seismic data. *Geophysics,* 48**,** 665–676.

FRANCIS, [illegible]imitations of deterministic seismic inversion data as input for reservoir model conditioning. SEG Technical Program Expanded Abstracts, 2010. Society of Exploration Geophysicists, 2396–2400.

FU, L.-Y. 2004. Joint inversion of seismic data for acoustic impedance. *Geophysics,* 69**,** 994–1004.

https://doi.org/10.5194/egusphere-2026-1391
Preprint. Discussion started: 8 May 2026

GOGOI, T. & CHATTERJEE, R. 2019. Estimation of petrophysical parameters using seismic inversion and neural network modeling in Upper Assam basin, India. *Geoscience Frontiers,* 10**,** 1113–1124.

GOLUB, G. H., HEATH, M. & WAHBA, G. 1979. Generalized cross-validation as a method for choosing a good ridge parameter. *Technometrics,* 21**,** 215–223.

GOODWAY, B., CHEN, T. & DOWNTON, J. 1997. Improved AVO fluid detection and lithology discrimination using Lamé petrophysical parameters;"λρ","μρ", & "λ/μ fluid stack", from P and S inversions. *SEG technical program expanded abstracts 1997.* Society of Exploration Geophysicists.

GYULAI, Á., BARACZA, M. K. & TOLNAI, É. E. 2013. The application of joint inversion in geophysical exploration.

HAAS, A. & DUBRULE, O. 1994. Geostatistical inversion-a sequential method of stochastic reservoir modelling constrained by seismic data. *First break,* 12.

HAN, J. & KAMBER, M. 2006. Data mining: concepts and techniques, 2nd. *University of Illinois at Urbana Champaign: Morgan Kaufmann*.

HASHEMI, H., JAVAHERIAN, A. & BABUSKA, R. 2008. A semi-supervised method to detect seismic random noise with fuzzy GK clustering. *Journal of Geophysics and Engineering,* 5**,** 457–468.

HORN, R. A. & JOHNSON, C. R. 2012. *Matrix analysis*, Cambridge university press.

https://doi.org/10.5194/egusphere-2026-1391
Preprint. Discussion started: 8 May 2026

JAFRI, M. K., LASHIN, A., IBRAHIM, E.-K. H., HASSANEIN, K. A., AL ARIFI, N. & NAEEM, M. 2017. Improved reservoir characterisation using fuzzy logic platform: an integrated petrophysical, seismic structural and poststack inversion study. *Exploration Geophysics,* 48**,** 430–448.

JAHANJOOY, S., RIAHI, M. A. & MOGHANLOO, H. G. 2022. Blind inversion of multidimensional seismic data using sequential Tikhonov and total variation regularizationsBlind seismic inversion using STTVR. *Geophysics,* 87**,** R53–R61.

KIEU, D. T. & KEPIC, A. 2020. Seismic-impedance inversion with fuzzy clustering constraints: An example from the Carlin Gold district, Nevada, USA. *Geophysical Prospecting,* 68**,** 103–128.

KRISHNAPURAM, R. & KIM, J. 1999. A note on the Gustafson-Kessel and adaptive fuzzy clustering algorithms. *IEEE Transactions on Fuzzy systems,* 7**,** 453–461.

LE, C. V., HARRIS, B. D., PETHICK, A. M., TAKAM TAKOUGANG, E. M. & HOWE, B. 2016. Semiautomatic and automatic cooperative inversion of seismic and magnetotelluric data. *Surveys in Geophysics,* 37**,** 845–896.

LI, B. N., CHUI, C. K., CHANG, S. & ONG, S. H. 2011. Integrating spatial fuzzy clustering with level set methods for automated medical image segmentation. *Computers in biology and medicine,* 41**,** 1–10.

LI, Y. & OLDENBURG, D. W. 1999. 3-D inversion of DC resistivity data using an L-curve criterion. 1999 SEG Annual Meeting, 1999. OnePetro.

https://doi.org/10.5194/egusphere-2026-1391
Preprint. Discussion started: 8 May 2026

LIAO, C., HU, X., ZHANG, S., LI, X., YIN, Q., ZHANG, Z. & ZHANG, L. 2022. Joint inversion of gravity, magnetotelluric and seismic data using the alternating direction method of multipliers. *Geophysical Journal International,* 229**,** 203–218.

LIU, Y. 2019. A comparison of Machine Learning methods for seismic inversion to estimate velocity and density. *GeoConvention 2019, Calgary, Canada***,** 13–17.

MAHALANOBIS, P. C. 2018. On the generalized distance in statistics. *Sankhyā: The Indian Journal of Statistics, Series A (2008-),* 80**,** S1–S7.

MALLICK, S. 1995. Model-based inversion of amplitude-variations-with-offset data using a genetic algorithm. *Geophysics,* 60**,** 939–954.

MAURYA, S. & SINGH, N. 2018. Comparing pre-and post-stack seismic inversion methods-a case study from Scotian Shelf, Canada. *J Ind Geophys Union,* 22**,** 585–597.

MAURYA, S., SINGH, N. P. & SINGH, K. H. 2020. *Seismic inversion methods: a practical approach*, Springer.

MENG, D., WU, B., WANG, Z. & ZHU, Z. 2021. Seismic impedance inversion using conditional generative adversarial network. *IEEE Geoscience and Remote Sensing Letters,* 19**,** 1–5.

MOOSAVI, N., BAGHERI, M., NABI-BIDHENDI, M. & HEIDARI, R. 2023. Porosity prediction using Fuzzy SVR and FCM SVR from well logs of an oil field in south of Iran. *Acta Geophysica,* 71**,** 769–782.

https://doi.org/10.5194/egusphere-2026-1391
Preprint. Discussion started: 8 May 2026

PHAM, D. L. 2001. Spatial models for fuzzy clustering. *Computer vision and image understanding,* 84**,** 285–297.

RAPSTINE, T. D. 2015. *Gravity gradiometry and seismic interpretation integration using spatially guided fuzzy c-means clustering inversion*, Colorado School of Mines.

ROSA, D. R., SANTOS, J. M., SOUZA, R. M., GRANA, D., SCHIOZER, D. J., DAVOLIO, A. & WANG, Y. 2020. Comparing different approaches of time-lapse seismic inversion. *Journal of geophysics and engineering,* 17**,** 929–939.

ROSA, D. R., SCHIOZER, D. J. & DAVOLIO, A. 2022. Enhancing vertical resolution with 4D seismic inversion. *Journal of Petroleum Science and Engineering,* 212**,** 110291.

RUDIN, L. I., OSHER, S. & FATEMI, E. 1992. Nonlinear total variation based noise removal algorithms. *Physica D: nonlinear phenomena,* 60**,** 259–268.

SUN, J. & LI, Y. 2016. Joint inversion of multiple geophysical and petrophysical data using generalized fuzzy clustering algorithms. *Geophysical Supplements to the Monthly Notices of the Royal Astronomical Society,* 208**,** 1201–1216.

TARANTOLA, A. 2005. *Inverse problem theory and methods for model parameter estimation*, SIAM.

TEREKHOV, A. V., PESIN, Y. B., NIU, X., LATASH, M. L. & ZATSIORSKY, V. M. 2010. An analytical approach to the problem of inverse optimization with additive objective functions: an application to human prehension. *Journal of mathematical biology,* 61**,** 423–453.

https://doi.org/10.5194/egusphere-2026-1391
Preprint. Discussion started: 8 May 2026

TIKHONOV, A. N., ARSENIN, V. J., ARSENIN, V. I. A. K. & ARSENIN, V. Y. 1977. *Solutions of ill-posed problems*, Vh Winston.

VAN DER BAAN, M. 2008. Time-varying wavelet estimation and deconvolution by kurtosis maximization. *Geophysics,* 73**,** V11–V18.

VERNIK, L. 2016. *Seismic petrophysics in quantitative interpretation*, Society of Exploration Geophysicists.

WANG, Y., JIA, Z. & LU, W. 2024. SEMI Net: Seismic-Electromagnetic Joint Inversion Network. *IEEE Transactions on Geoscience and Remote Sensing,* 62**,** 1–15.

YILMAZ, Ö. 2001. *Seismic data analysis: Processing, inversion, and interpretation of seismic data*, Society of exploration geophysicists.

YU, B., ZHOU, H., WANG, L. & LIU, W. 2020. Prestack Bayesian statistical inversion constrained by reflection features. *Geophysics,* 85**,** R349–R363.

YU, S. & MA, J. 2021. Deep learning for geophysics: Current and future trends. *Reviews of Geophysics,* 59**,** e2021RG000742.

ZADEH, L. A. 1965. Fuzzy sets. *Information and control,* 8**,** 338–353.

ZHANG, J., LI, J., CHEN, X., LI, Y., HUANG, G. & CHEN, Y. 2021. Robust deep learning seismic inversion with a priori initial model constraint. *Geophysical Journal International,* 225**,** 2001–2019.

https://doi.org/10.5194/egusphere-2026-1391
Preprint. Discussion started: 8 May 2026

ZHANG, R. & FOMEL, S. 2017. Time-variant wavelet extraction with a local-attribute-based time-frequency decomposition for seismic inversion. *Interpretation,* 5**,** SC9–SC16.

585 ZHDANOV, M. S., GRIBENKO, A. & WILSON, G. 2012. Generalized joint inversion of multimodal geophysical data using Gramian constraints. *Geophysical Research Letters,* 39.

https://doi.org/10.5194/egusphere-2026-1391
Preprint. Discussion started: 8 May 2026

Figures

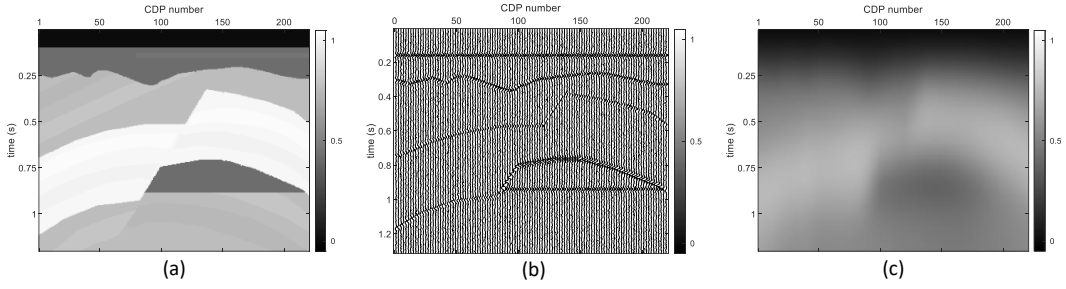

Figure 1. Synthetic Model. (a) Natural logarithm of the AI model. (b) seismic section. (c) Initial model.

590

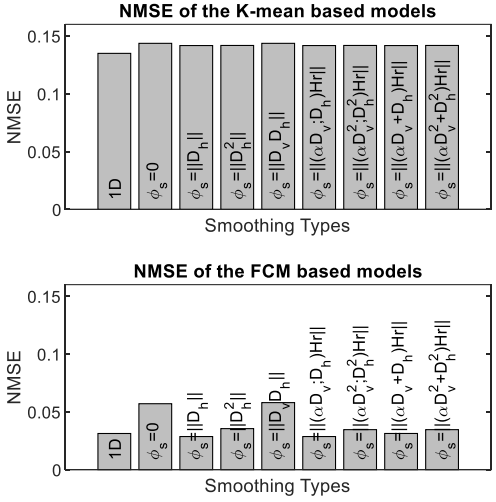

Figure 2.Normalized mean square error of the result models using different smoothness terms. K-means is used as the term (upper plot). FCM is used as the term (lower plot).

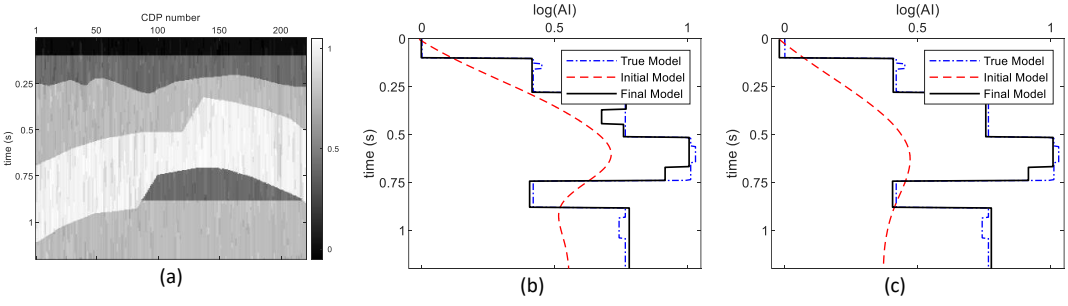

595 **Figure 3. (a) Calculated AI models using the first difference matrix and prior information. (b) and (c) A log at the location of trace 100 and the result using different initial models.**

https://doi.org/10.5194/egusphere-2026-1391
Preprint. Discussion started: 8 May 2026

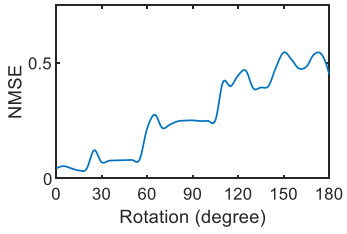

Figure 4. NMSE of the resulting model for trace 100 using incorrect phase rotation of the Ricker wavelet.

600

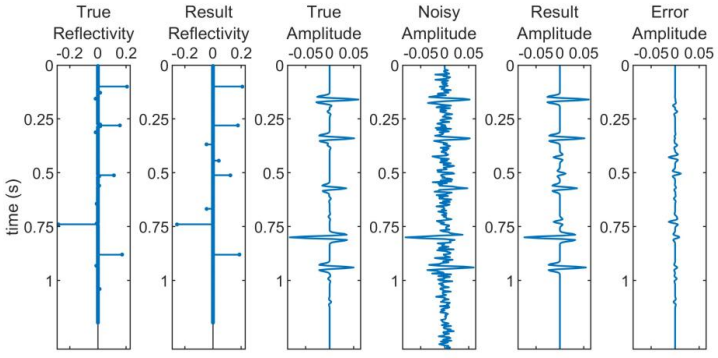

Figure 5. True and calculated data at the location of CMP 100 of the synthetic data.

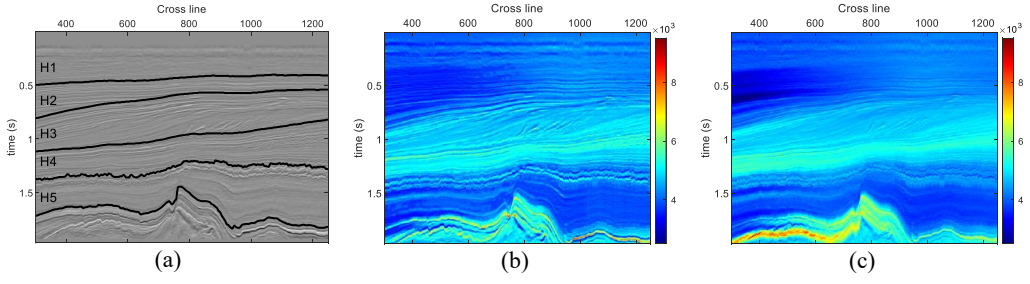

Figure 6. Seismic section of Inline 441, F3 Block and five interpreted horizons (b) Inversion result of the third approach of the proposed method. (c) Model-based inversion (HR).

605

https://doi.org/10.5194/egusphere-2026-1391
Preprint. Discussion started: 8 May 2026

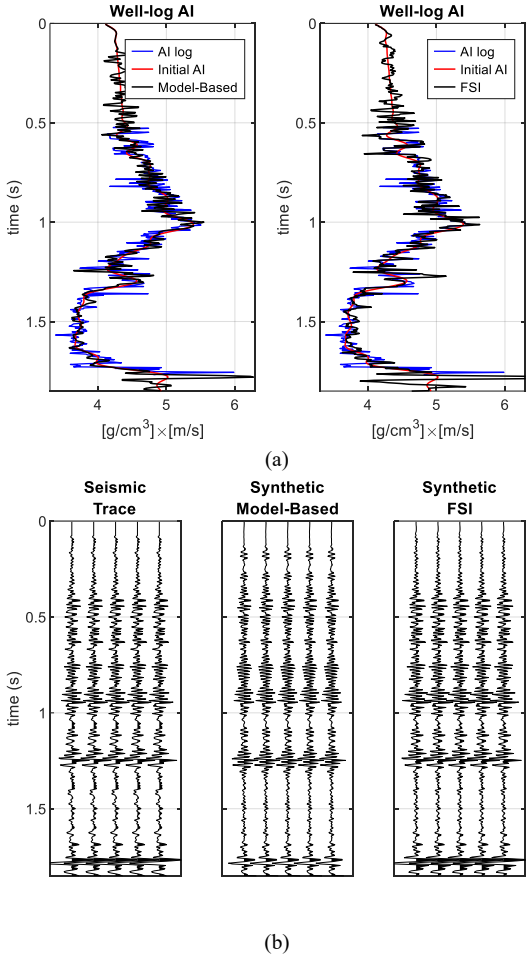

Figure 7. Acoustic Impedance at the intersection of inline 441 and crossline 1008 in the location of the well F034, F3 Block data. (a) FSI. (b) Model-Based.

610

https://doi.org/10.5194/egusphere-2026-1391
Preprint. Discussion started: 8 May 2026

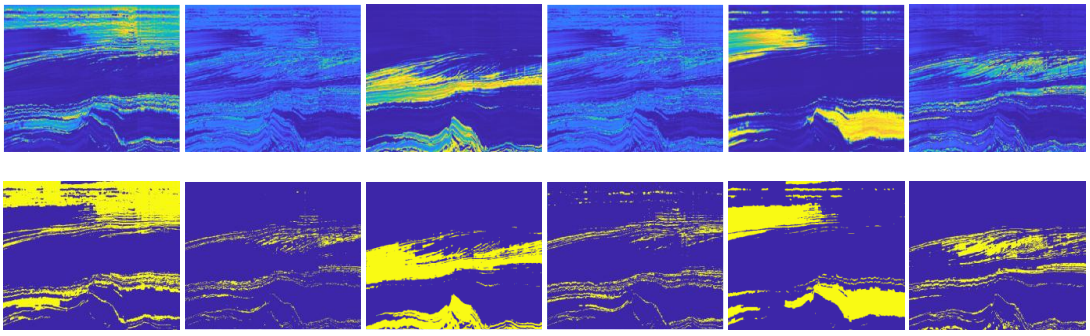

Figure 8. Membership sections of Figure 6. b in which q=2 (upper row). Membership sections of the same inversion while q=1.1(lower row).

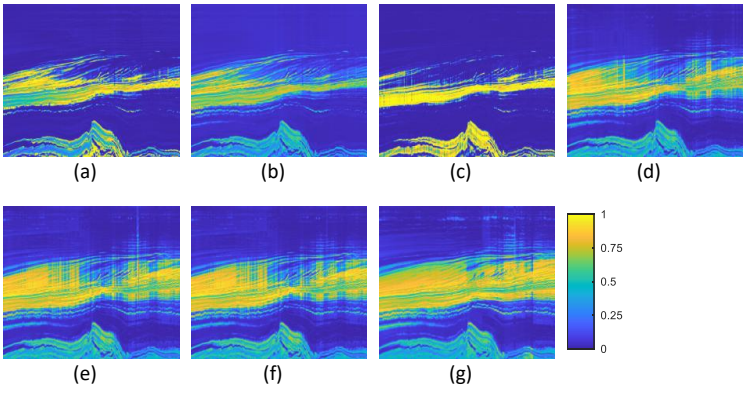

Figure 9. Membership sections comparable to Figure 7 in different situations of initial data and updating clusters. (a) Initial model and clusters, fixed AI of the centroids. (b) Initial model and clusters, fixed AI, and times of the centroids. (c) Initial model and clusters, updating 1D AI of the centroids. (d) Initial model and clusters, updating AI and times of the centroids. (e) Initial model, no initial clusters, updating AI and times of the centroids. (f) No initial model, initial clusters, updating AI, and times of the centroids. (g) No initial model, no initial clusters, updating AI and times of the centroids.

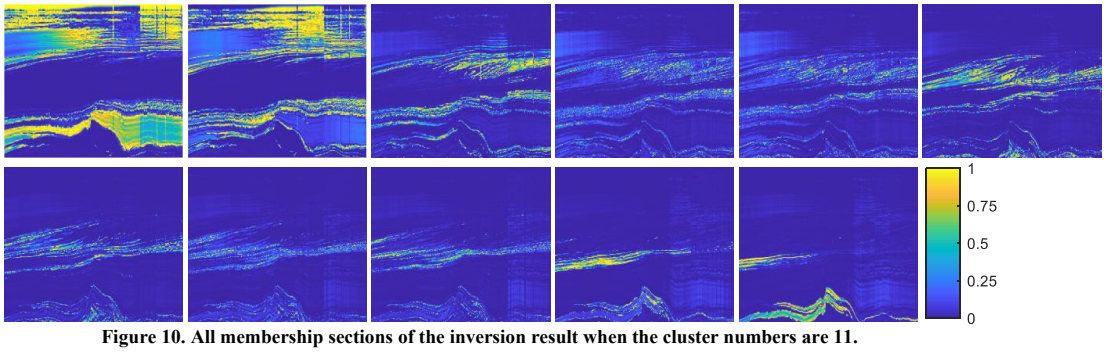

Figure 10. All membership sections of the inversion result when the cluster numbers are 11.